Wind Tunnel Investigation of Low-Speed Buffeting of the Pioneer Venus Probes

Trevor C. Sorensen*
NASA Ames Research Center, Moffett Field, Calif., and
Center for Research Inc., University of Kansas, Lawrence, Kansas
and
Vincent U. Muirhead†
Center for Research Inc., University of Kansas, Lawrence, Kansas

A wind-tunnel investigation was conducted to evaluate the effectiveness of possible modifications to the Pioneer Venus probes to reduce buffeting due to aerodynamic force fluctuations. The tests were conducted at Reynolds numbers of 2×10^5 to 9×10^5 based on pressure sphere diameter. Force fluctuations were found to be strongly dependent on Reynolds number, decreasing by a factor of 3 in the range tested. A screen ring at the forced separation point was highly effective in reducing the force and pressure fluctuations by up to a factor of 4. No evidence was found for a discrete Strouhal number of regular fluctuations from vortex shedding.

Introduction

IN 1978, NASA is planning to send Pioneer spacecraft to Venus. The purpose of the Pioneer Venus Project is to make cost-effective extensions of our present knowledge of Venus.[1] The multiprobe mission will include one large and three small probes that will descend through the Venusian atmosphere and hard-impact on the planet's surface. During descent, the probes will investigate the Venusian atmosphere: its composition, circulation, cloud structure, thermodynamics, and interaction with solar emissions.

In order to obtain accurate results from these experiments, particularly measurements of atmospheric turbulence, it is desired that the probe descent be steady. However, bluff bodies passing through the atmosphere at low subsonic speeds, as would be encountered on the Pioneer mission before impact, are subject to buffeting due to the unsteady flow over the body. Such buffeting was experienced in low-speed descent by the Planetary Atmosphere Experiments Test (PAET) probe,[2] which demonstrated atmospheric measurements during high-speed entry and descent of a probe in the Earth's atmosphere. Although the buffeting did not interfere seriously with the PAET determination of atmosphere structure, it is undesirable, particularly in a deep atmosphere such as that of Venus where low-speed descent will occur for a time period of about an hour, and, as just noted, buffeting clearly will interfere with attempts to measure atmospheric turbulence.

In order to investigate the magnitude of buffeting associated with the Pioneer Venus probe geometries and to seek ways of suppressing it, the Flight Research Laboratory at the University of Kansas conducted a wind tunnel investigation of the buffeting problem due to aerodynamic influences. Although the atmosphere of Venus is predominantly carbon dioxide and is also much denser than the Earth's atmosphere, it was desirable to see what improvements could be accomplished for low subsonic Mach numbers and Reynolds numbers using an environment with which it is easy to work (air). Results and trends would be noted, and then potentially favorable modifications could be tried at the actual Reynolds numbers that are expected. This paper presents the results of the investigation in air at low Reynolds numbers.

Presented as Paper 77-321 at the AIAA 13th Annual Meeting and Technical Display Incorporating the Forum on the Future of Air Transportation, Washington, D.C., Jan. 10-14, 1977; submitted Jan. 28, 1977; revision received Aug. 30, 1977.

Index categories: Entry Vehicle Dynamics and Control; Entry Vehicle Testing, Flight and Ground; Entry Vehicles and Landers.

*Space Science Division; formerly Research Assistant, Center for Research Inc. Member AIAA.

†Professor of Aerospace Engineering. Member AIAA.

Theoretical Considerations

The wake behind circular cylinders is basically unsteady and contains distinct vortices. These vortices are alternately clockwise and counterclockwise and are shed by the cylinder at regular intervals. This phenomenon has been studied extensively for the subcritical flow regime and has been shown to have a definite relationship expressed by the Strouhal number

$$S=fd/V\simeq 0.22 \tag{1}$$

where f is the shedding frequency, d is the cylinder diameter, and V is the airstream velocity.

The vortex shedding on alternate sides of the cylinder causes a harmonically varying force on the cylinder in a direction perpendicular to that of the airstream. The cylinder thus oscillates with the same frequency as that at which the vortices are shed.[3] However, in the supercritical region, regular vortex shedding is not obvious and has not been observed at all by many investigators. Some have observed velocity pulsations for Reynolds numbers (R_N) of 3×10^6 giving higher values of S than in subcritical flow for higher R_N. Pressure measurements on the cylinders show periodic fluctuations only at points located ahead of the boundary-layer separation point. Points behind the separation point show an entire frequency spectrum caused by the strong turbulent region in the wake. The Strouhal number obtained from the pressure measurements ahead of the separation point has been approximately 0.2 for various R_N in the supercritical region.

In the three-dimensional case, much research has been done on spheres in wind tunnels and freestream, both in flight and in ballistic ranges. The drag, static pressure distribution, boundary-layer transition and separation, and wake turbulence have been investigated and documented thoroughly. However, little research has been done on the nature of vortex shedding and methods of suppressing the resultant buffeting.[4]

Buffeting is a result of pressure disturbances caused by the unsteady flow on the surface of the body associated with flow

separation and turbulent flow from the vortex shedding. Thus, it would appear to be an inevitable consequence of separated base flow. However, the intensity would be expected to depend on certain features subject to design control, such as fixing the separation line vs letting its location be free. In order to steady the flow around the body, the forward stagnation point also must be fixed. Furthermore, the unsteady force level should be reduced by minimizing the size of the vortices shed, and the regularity could be improved by making the shedding as uniform as possible.

The basic Pioneer probe configurations are designed to provide aerodynamic braking to slow their descents. In the wind-tunnel program reported herein, the buffeting of the basic probe configurations was measured, and modifications of probe geometry designed to suppress the buffeting were tested. To be acceptable, any modification was required to have a drag coefficient as high as the original configuration in order to maintain the desired degree of aerodynamic braking.

The modifications included were designed to do the following: 1) steady the stagnation point by using a small cone or protrusion on the nose of the probe model; 2) channel and steady the flow before the separation point by using fences or vortex generators; 3) minimize the scale and steady the vortex shedding from the separation point by using a screen ring, porous flanges, or box vanes at the separation point, and bleed air collected from a hole in the nose, channeled underneath the shield and injected into the turbulent region behind the separation point (or in some configurations before the separation point); and 4) steady the air flow in the turbulent wake by using a central vent to channel air from an intake in the nose to a rear annulus, where the air is injected into the turbulent flow region. The bleed air behind the separation point also was expected to help steady the turbulent wake.

Reference 5 indicates that the use of a porous ring at the separation point can improve the dynamic motion of a sphere, as experienced in buffeting. During this investigation, lift, drag, and side-force measurements were made at Mach numbers from 0.063 to 0.260 on 29 modifications of the probe models in the University of Kansas 0.914×1.29-m wind tunnel at Reynolds numbers of 2×10^5 to 9×10^5 based upon the pressure sphere diameter. The wind tunnel has a turbulence factor of less than 1.1 (ratio of free-flight to wind-tunnel transition Reynolds numbers), which indicates relatively low turbulence.[6] The tests concentrated mainly on the modified large-probe configurations, and spin tests were made on some of the models. Pressure measurements were made at selected points on the surface of the probe configurations. Both the mean values and fluctuations of the test parameters were recorded.

The details and test results for the unmodified probes and the most successful modifications are presented in this paper. Complete details and results for all of the models tested are available in Ref. 7.

Description of Equipment

Probe Models

The standard unmodified large- and small-probe models are shown in Figs. 1a and 1b, respectively. Common to both models was a 15.24-cm-diam pressure sphere that was mounted on the sting. The sphere consisted of two hemispheres of spun brass attached with screws to a central aluminum mounting wheel. At the center of the mounting wheel was a tubular roller bearing, which fitted on the end of the 1.11-cm steel sting mount. The wheel was locked in place using a lock washer and nut. For spin tests, the lock washer was removed, and the model then was free to rotate about the sting. For tests requiring pressure measurements, a hollow sting was used, allowing the pressure transducer leads to pass through. The sphere contained 21 equally spaced (radially) holes for the installation of the miniature pressure transducers.

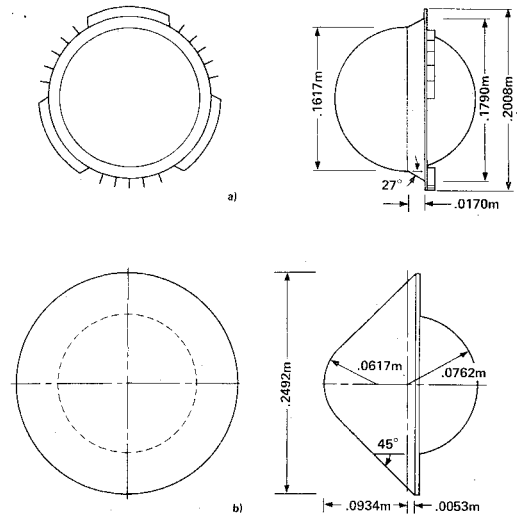

Fig. 1 Standard probe models: a) large probe; b) small probe.

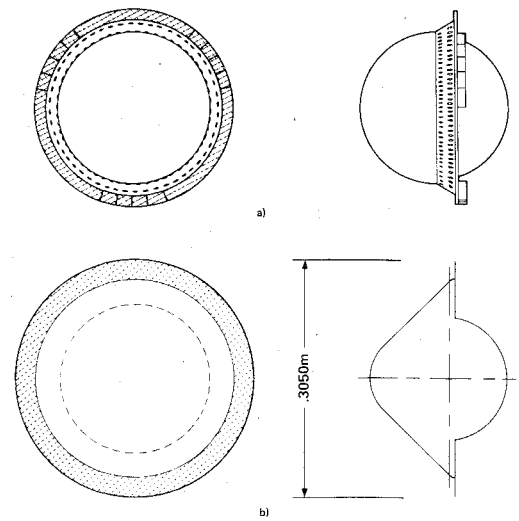

Fig. 2 Modified probe models: a) large probe; b) small probe.

Large Probe

The large probe consisted of a basic 16.17-cm-diam spun-brass hemispherical shield mounted on the front half of the pressure sphere, leaving a spacing of 0.47 cm between them. The shield used for pressure measurement tests contained 13 equally spaced holes for the transducers. Any holes without transducers were plugged using the bolts protruding from the pressure sphere and smoothed with clay. The shield was attached to a 27-deg sloped aluminum flange or solid ramp, behind which was a 60-deg sector brass ring divided into six parts, three with solid sectors and three with spin vanes. The three solid sectors were to act as speed brakes to slow the probe descent, while the areas with vanes were to provide spin for averaging out aerodynamic asymmetry and to meet instrument sampling requirements.

The modified large probe (Fig. 2a) had a porous ramp at the forced separation point consisting of one row of 152 holes 1.86 mm in diameter parallel to the probe spin axis, and another row of 148 holes 1.52 mm in diameter. Behind the ramp was a screen ring, which replaced the 60-deg solid disk sector ring of the large probe. The ring was 20.08 cm o.d. and extended radially 1.09 cm or about 13.5% of the nose shield radius beyond the ramp maximum diameter. The screen was plain-weave stainless-steel wire cloth of 14 mesh/linear 2.54 cm. The wire diameter was 0.457 mm, the opening 1.346 mm, and the open area 55.1%. A 20.08-cm-diam wire ring was attached around the outer diameter of the screen area to

provide stiffness. The vane ring without solid sectors was attached behind the screen ring to provide spin.

Small Probe

The small probe (Fig. 1b) consisted of a spun-brass shield covering the front half of the pressure sphere with a maximum diameter of 24.92 cm. The shield used for the pressure measurements had eight holes near the rear of the shield for pressure transducer installation.

The modified small probe (Fig. 2b) had a screen ring attached behind the shield, extending from the surface of the pressure sphere to a maximum diameter of 30.5 cm, with a radial extension of 2.9 cm or 22.4% of the shield base radius. The screen ring was the same mesh as that used for the modified large probe.

Model Sting Mounts

Three different mounting stings were made for the tests. The first sting was 61-cm-long steel tubing (4 model diam long to center of sphere) and varied in diameter from 1.27 cm entering the model to 2.54 cm at the rear. Because of poor stiffness and damping characteristics, this sting was not used past the initial tests.

The second sting used was 22.9-cm-long steel tubing (1½ diam long from sphere center) and was 1.429 cm in diameter for the entire horizontal section. The horizontal section was welded to a 1.91-cm-diam vertical solid steel rod, which was mounted in the balance table mount. The horizontal sting tube was hollow to allow passage for the pressure transducer leads. Both the horizontal and vertical sections were strain-gaged to obtain force measurements when the balance table was locked.

The third sting used had the same external dimensions as the second sting and was designed to obtain force measurements from strain gages and especially to obtain accurate drag readings without the interference of the lift and side forces, as occurred with the second sting. The horizontal section was not hollow, and thus no pressure measurements were taken using this sting. The sting sections coming from the model mounting wheel and from the vertical mount met inside the rear half of the pressure sphere (Fig. 3) and were joined by two vertical steel plates, one measuring $1.9\times8.9\times0.0159$ cm and the other $1.9\times8.9\times0.93$ cm. The two plates were attached to each other at the ends by single bolts, which passed through horizontal bar spacers that left a gap of 0.65 cm between the plates. The thinner plate was strain-gaged to provide the drag measurements. For all of the stings, there was a wind shield around the vertical section to reduce erroneous readings due to aerodynamic forces acting on the sting.

Instrumentation

Force measurements were obtained by three different methods:

1) The mean values of lift, drag, and side force were obtained one at a time from the three force components of the six-component strain-gaged wind-tunnel balance (the three moment components were not measured) and shown on the meter of a microvolt indicating amplifier, from which the values were recorded.

2) The output from the balance also was connected to a data acquisition system and then to a visicorder, where the analog outputs of the three forces were recorded simultaneously on 20.3-cm direct print visicorder paper.

3) Simultaneous analog outputs of lift, drag, and side force were obtained from strain gage bridge circuits attached to the stings with the wind-tunnel balance locked and were run through the preceding data acquisition system to be recorded on the visicorder paper.

The repeatability of the visicorder force data was about ±0.01% of the full-scale reading but varied slightly depending on the acquisition channel used. The data obtained from the strain gages mounted on the sting are considered to be less accurate than the balance data because of possible electric shielding and interference effects. The accuracy of the force coefficients from the gage data is estimated to be about ±5% based on comparison of results from the other methods, whereas the accuracy of the balance force coefficients is ±3%.

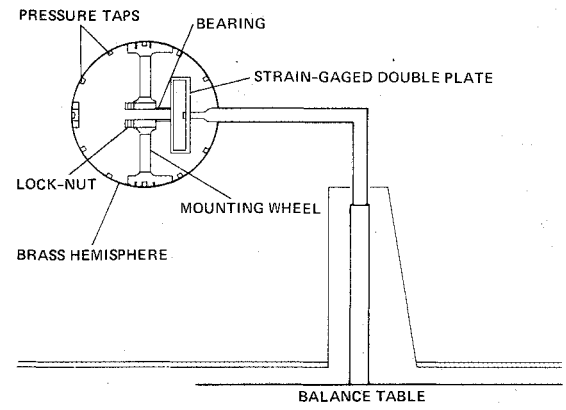

Fig. 3 Mount system with the drag-plate sting.

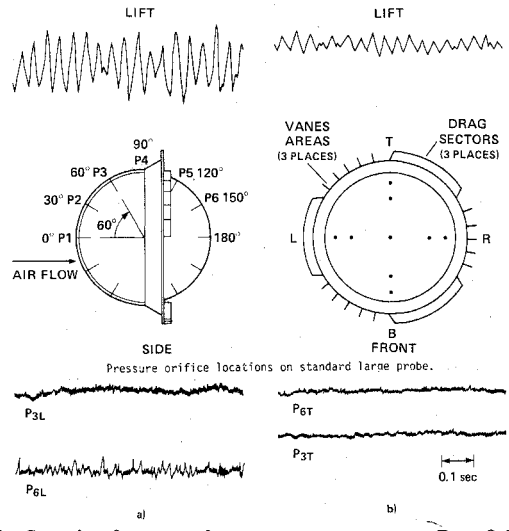

Fig. 4 Sample force and pressure traces at $R_N \simeq 8.5\times10^5$: a) standard large probe; b) modified large probe.

Mean pressure values on the model surface were obtained by running plastic tubing from the transducer holes through the sting to an alcohol manometer, from which the readings were recorded. Pressure fluctuations as well as mean values were measured by flush-mounted 0.3175-cm-diam absolute pressure transducers. The subminiature transducers were bonded semiconducter bridge-type gages with temperature compensation. The analog outputs from the transducers were recorded on visicorder paper after being processed and amplified by the data acquisition system, as described previously. The transducers had a sensitivity of 0.0014 mV/(N/m^2) and a repeatability of 0.25% of full scale during static calibration tests. The pressure fluctuation coefficients (ΔC_p) have an accuracy of ±5%. The wind-tunnel static and dynamic pressures also were measured from alcohol manometers. Wind-tunnel test section temperature was read from a thermometer mounted in the tunnel wall.

Test Procedures

Frequency Responses

The natural frequencies and damping characteristics of the models mounted on the various stings were determined at no

flow by applying a nearly instantaneous impulse for lift, drag, and side force in turn and recording the output on the visicorder. In order to obtain system responses to known cyclic inputs, the models were subjected to a controlled longitudinal periodic force in each of the three force directions. The amplification factors for lift, drag, and side force due to system resonance thus obtained showed the expected strong dependence on frequency.

Tests

Each probe model was tested at four or seven air speeds between 22.3 and 89.4 m/sec (Mach numbers from 0.063 to 0.260). Each configuration was tested with the model locked to the sting mount so that it could not spin about its longitudinal axis. The standard and modified large probes also were tested with the models free to spin. The free airflow-induced spin rates of the models during the tests were determined using a stroboscope. The models were tested at zero incidence.

Results and Discussion

Treatment of Data

The fluctuation force coefficients were calculated from traces such as those in Fig. 4 using the maximum amplitudes of the output vibrations as recorded on the visicorder paper. In most cases, the recorded output frequency was very near the natural frequency of the measuring mount system. The sting mount acted as a mechanical filter amplifying the vibration amplitudes at the natural frequencies relative to those of other frequencies. In order to obtain amplitudes of the forcing vibrations, it was necessary to allow for the amplification effect at the natural frequency of the mount system. The amplification factor μ is the ratio of the apparent force to the actual input force level at a given frequency:

$$\mu = F_{\text{apparent}} / F_{\text{input}} \qquad (2)$$

The reported values of the force coefficient fluctuations, divided by the amplification factor ($C_{L,D,SF}/\mu$), represent a lower limit on the actual buffeting force variations and are interpreted to be that part of the force fluctuations having a frequency near the support system natural frequency.[7] The effectiveness of this method in accounting for sting mechanical interference effects is shown by the fact that there was close correlation ($\pm 5\%$) between the force fluctuation coefficients obtained from the different sting mounting systems used, even though their natural vibration characteristics were quite different.

The configurations initially were compared using the maximum amplitudes of fluctuation for convenience. From those comparisons, the best configuration was chosen for both the large and small probes. To give a better indication of the amount of fluctuation suppression provided by the two modified configurations as compared to the standard configurations, a standard deviation analysis was done. The visicorder data were digitized and then reduced. The results using this method correlated well with those that used maximum amplitudes only.

An autocorrelation and power spectral density analysis also was tried on these data, but the resolution possible with the equipment available was not fine enough to give any useful results. The pressure transducer traces on the visicorder paper were corrected to account for the internal noise, which caused a wider trace than in a noise-free system. The useful amplitude of the fluctuations thus was determined after subtracting the initial trace width (with tunnel not running) from the maximum recorded trace amplitude.

Comparison of Measured Force Fluctuation Levels

The mean drag and drag fluctuations of the standard and modified large-probe models are shown in Fig. 5, and the spin

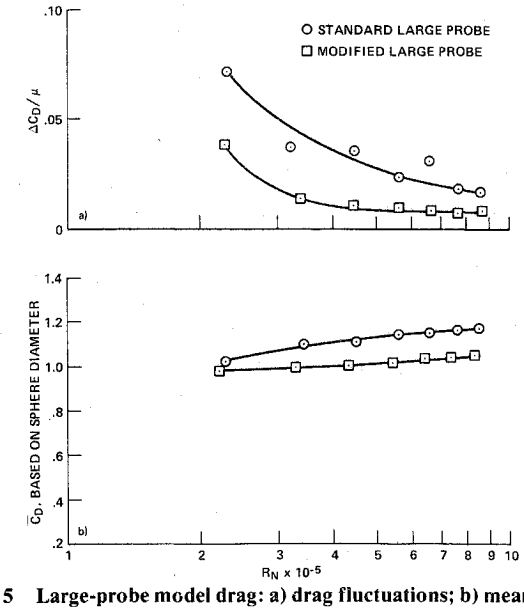

Fig. 5 Large-probe model drag: a) drag fluctuations; b) mean drag.

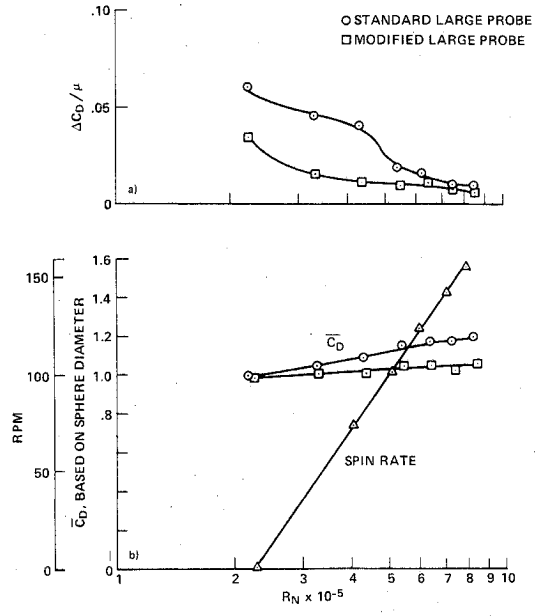

Fig. 6 Large-probe model drag (spinning): a) drag fluctuations; b) mean drag.

test drag results are shown in Fig. 6. The mean drag levels of the modified large-probe model were about 10% less than the basic probe model. The matching of drag coefficients easily could be made closer by increasing the drag screen area. The standard large-probe model exhibited drag fluctuations conservatively placed at up to 7% of the mean drag level. Buffet levels were reduced with the screen by factors of 2 to 4. Buffeting of the unmodified probe also appears to depend on spin. (Compare Figs. 5 and 6 at the higher R_N.) For the small probe (Fig. 7), the screen addition increased drag by about 25%, whereas it reduced buffet levels by as much as a factor of 4. The buffeting intensity and its reduction ratios appear to be strongly Reynolds number dependent, decreasing by a factor of about 3 in the range tested.

The fractional fluctuation of the drag coefficients ($\Delta C_D/\mu\bar{C}_D$) is plotted in Fig. 8 for the large probe. Similarly, the lift and side-force fluctuations relative to the mean drag coefficient are plotted in Figs. 9 and 10. From these graphs, it is noted that the large-probe configuration with screen ring has as little as 1% drag fluctuation compared to the 2 to 3% for the standard model.

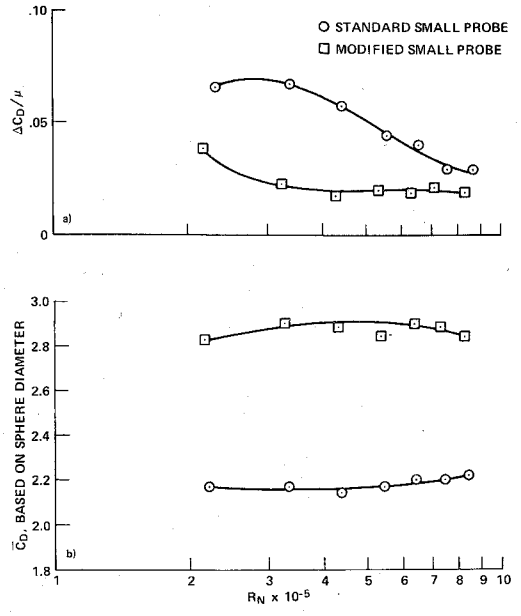

Fig. 7 Small-probe model drag: a) drag fluctuations; b) mean drag.

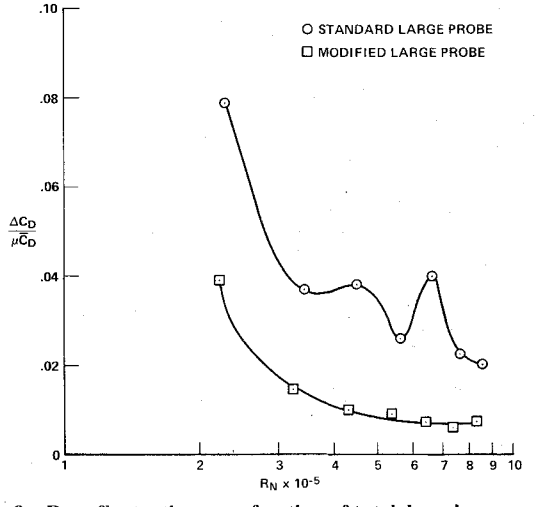

Fig. 8 Drag fluctuations as a fraction of total drag: large probe.

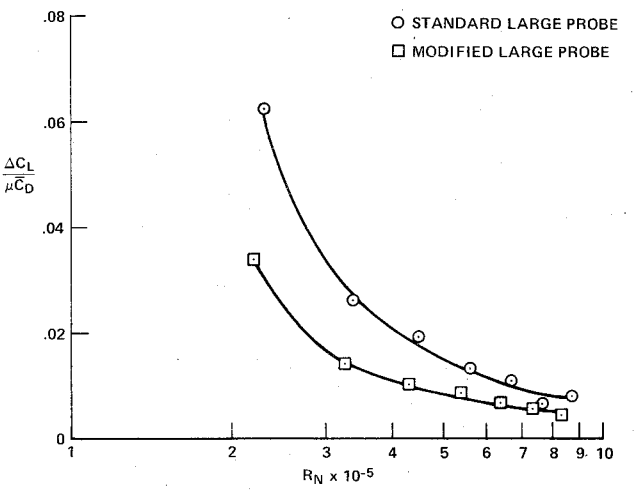

Fig. 9 Lift fluctuations as a fraction of total drag: large probe.

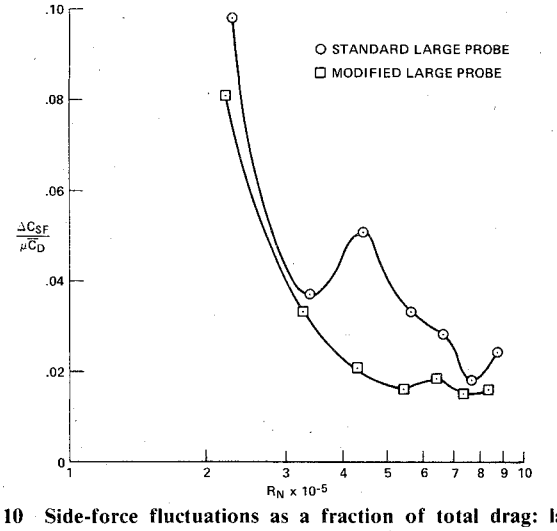

Fig. 10 Side-force fluctuations as a fraction of total drag: large probe.

Fluctuations in lift and side force followed patterns similar to the drag fluctuation. Differences between ΔC_L and ΔC_{SF} for the standard probe may be real, as the three drag-plate sectors are rotated relative to the force axes and are not the same for C_L and C_{SF}. For the modified configuration, the only asymmetry was in the placement of the three groups of spin vanes. In addition, it should be realized that the sting stiffness and natural frequency differ in the two planes.

Although the modified large probe discussed had a porous separation ramp as well as the screen ring, the effectiveness of the ramp porosity in reducing buffeting was small in comparison with the screen ring. For the effect of the porous ramp alone, as well as the effectiveness of the other modifications tried (such as nose shield holes, vortex generators, etc.), the reader is referred to Ref. 7.

Pressure Fluctuations on Model Surface

Mean pressure coefficients ($\bar{C}_p$) for the standard large- and small-probe models, as measured on the alcohol manometer at a Reynolds number of 8.6×10^5, are shown in Fig. 11b. Pressure fluctuations (ΔC_p) obtained from the bonded pressure transducers are shown in Fig. 11a for the standard and modified large-probe models. The pressure traces obtained show a relatively steady stagnation pressure on the probe models. The local static pressures ahead of the separation point ($\theta = 30$, 60 deg) were relatively steady, except for the $\theta = 60$-deg locations ahead of the solid drag sectors, as shown by trace P_{3L} for the standard probe in Fig. 4. The fluctuation coefficients in Fig. 11a show the contrast between this unsteadiness and the relatively smooth traces obtained from in front of the vaned sectors. Behind the separation point, the pressure traces show the unsteadiness of the turbulent region (traces P_{6L} and P_{6T} in Fig. 4). The traces behind the 60-deg solid ring sectors show some additional large-scale disturbances present in the wake of the drag plate, above that of the basic turbulent wake pattern.

The presence of the screen ring reduced the random pressure fluctuations in the wake region by as much as 50%. An example of the effect of the screen ring and porous ramp is shown clearly in Fig. 4 by comparing the trace P_{6L} of the standard probe model with the trace P_{6T} of the modified large probe.

It was intended to do a detailed vibration analysis of the pressure output to determine whether a regular periodic vibration was present, as could be expected if there was regular vortex shedding or if fluctuations were purely random as encountered in true turbulent flow. However, digital output recording difficulties precluded a detailed analysis, and only a qualitative evaluation was made. The conclusion of this evaluation was that there were no sustained periodicities apparent in the pressure traces and thus no evidence of regular vortex shedding.

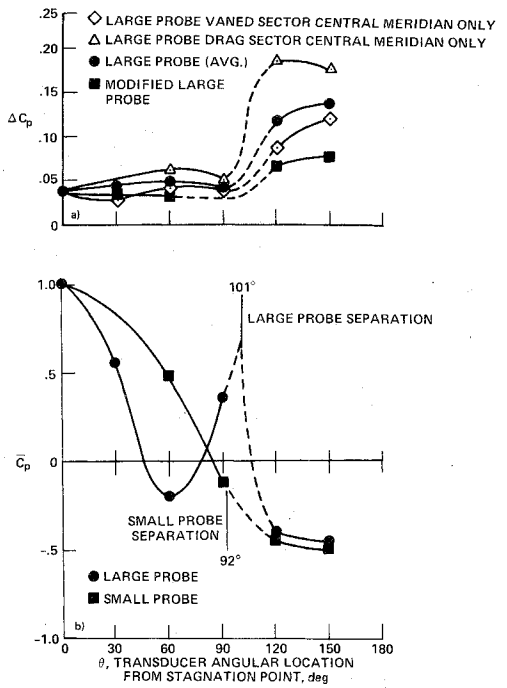

Fig. 11 Pressure coefficients at $R_N = 8.5 \times 10^5$: a) fluctuations in C_p for large-probe models; b) $\bar{C}_p$ for standard probe models.

Mounting System Interference Considerations

The force vibrations appeared in most cases at the natural vibration frequency of the mounting system, a phenomenon sometimes called self-excited vibration. According to Ref. 8, for systems with damping force that is very small in comparison to the elastic and inertia forces of motion, the frequency of the self-excited vibration is very near that of the system natural frequency. The damping in all systems used in the tests was very small (<0.03). Self-excited vibration cannot exist without an extraneous source of energy, and in most cases the source is nonperiodic (such as random turbulence). It was considered that the self-excitation might be due to configuration aerodynamics, but this was ruled out since the damping of the probes was positive. The dynamics of the probe-mount system translates the energy from a random force input into a self-excited vibration. The probe and sting in an air flow, being pivoted about a point behind the model base, tend to diverge laterally (reverse weather-cocking). This motion continues until the aerodynamic and inertia forces are overcome by the spring force of the sting, and the motion is reversed. This type of self-excited oscillation appears at the natural frequency of the system, just as was observed in the force traces. The excitation, however, ultimately requires an unsteady aerodynamic force applied to the model to sustain the oscillation.

Since forced vibrations in the steady state have the same frequency as the external (forcing) alternating source, any significant alternating force acting on the model should be visible on the output traces at its own frequency. Furthermore, periodic forcing vibrations not due to the mounting system or tunnel vibration should show as a common frequency in the data taken for the same configuration using different mounting systems. Although no such common vibration frequencies were observed in the traces, an unexplained frequency of about 2 Hz did appear in some drag traces for the standard large-probe model. Although inconclusive, this could be a buffeting vibration, since it matches closely the drag buffeting frequency obtained from the drop test of a large-probe model at the NASA Ames Research Center in 1974.[9] Generally, though, it appears that aerodynamic buffeting forces of identifiable frequency acting on the wind-tunnel models were too weak to overcome the inertial and elastic forces of the sting-mount systems.

Conclusions

The standard large-probe models exhibited drag fluctuations up to 7% of the mean drag levels. The three 60-deg solid ring sector drag plates mounted to the separation ring produced fluctuations ahead of the separation ring and additional fluctuations behind the ring in the turbulent area. A drag screen at the separation point was the most effective way found for suppressing fluctuations. The force and pressure fluctuations were suppressed up to a factor of 4 by the use of these screens in place of the drag plates at maximum diameter stations and by making the separation flange porous, if present. The screen acts to reduce the size of the shedding vortices, so that a more homogeneous turbulent separated flow is created. The fluctuation levels for all configurations depended strongly on Reynolds number and decreased by a factor of about 3 as the Reynolds number increased from 2×10^5 to 9×10^5.

Although a possible drag buffeting frequency for the standard large-probe model of about 2 Hz was found, generally, the aerodynamic buffeting forces were too weak to be distinguishable from the mount systems' natural frequencies. No evidence was found, from either the force or pressure traces, for a discrete Strouhal number of regular fluctuations from vortex shedding.

Acknowledgment

This work was conducted under Contract NAS2-8556, sponsored by the NASA Ames Research Center. The advice and comments of Alvin Seiff, who was the program technical monitor, are gratefully acknowledged.

References

[1] Dyer, J., Nunamaker, R., Cowley, L., and Jackson, R., "Pioneer Venus Mission Plan for Atmospheric Probes and an Orbiter," *Journal of Spacecraft and Rockets,* Vol. 11, Oct. 1974, pp. 710-715.

[2] Seiff, A., Reese, D., Sommer, S., Kirk, D., Whiting, E., and Niemann, H., "PAET, An Entry Probe Experiment in the Earth's Atmosphere," *Icarus,* Vol. 18, 1973, pp. 525-563.

[3] Kovasznay, L.S.G., "Hot-Wire Investigation of the Wake Behind Cylinders at Low Reynolds Numbers," *Proceedings of the Royal Society* (London), Vol. A198, 1949, pp. 174-190.

[4] Goldburg, A. and Florsheim, B.H., "Transition and Strouhal Number for the Incompressible Wake of Various Bodies," *The Physics of Fluids,* Vol. 9, Jan. 1966, pp. 45-50.

[5] Cahen, G.L., "Effects of Porous Rings on the Aerodynamic Characteristics of a Sphere," *Journal of Spacecraft and Rockets,* Vol. 12, Sept. 1975, pp. 572-574.

[6] Pope, A., *Wind Tunnel Testing,* 2nd ed., Wiley, New York, 1954, pp. 105-109.

[7] Muirhead, V.U., "Investigation of the Probe Buffeting Problem at Low Subsonic Mach Numbers," Flight Research Lab., University of Kansas, Lawrence, Kansas, Rept. FRL 500, July 1975.

[8] Den Hartog, J.P., *Mechanical Vibrations,* McGraw-Hill, New York, 1956, pp. 283-306.

[9] Seiff, A., private communication, 1974.